Available online at www.sciencedirect.com

ScienceDirect

Energy Procedia 77 (2015) 665 – 676

Energy Procedia

5th International Conference on Silicon Photovoltaics, SiliconPV 2015

Doping level effect on sample temperatures in infrared belt furnace firing

Evert E. Bende, John Anker

ECN – Solar Energy, Westerduinweg 3, 1755 LE, Petten, The Netherlands

Abstract

A firing study has been conducted for a variety of samples with different surface morphologies as well as with different bulk and emitter doping concentrations. In this study the firing settings were fixed and the temperature profile on the sample was measured with thermocouples. We have observed that the measured peak temperature on solar-cell R&D samples in an infrared (IR) conveyer belt firing furnace is strongly dependent on the surface morphology of the sample and its doping level. The surface morphology determines the coupling of IR radiation into the substrate. Samples with a random pyramids (RP) surface texture have reached temperatures that were 150°C higher than that of their polished counterparts. In addition to that, the doping level determines the free carrier absorption (FCA) and thus the heating up due to absorption of IR radiation. We have derived an analytical expression for a Planck-spectrum weighed FCA coefficient that is inversely proportional with the absolute black-body temperature (T) squared. Since the total energy radiated by a black body scales with T^4, the radiation absorption is proportional with T^2. The total doping level of a sample was quantified by G_{tot}, the summation of the sheet conductance values [Ω^{-1}/sq] of the base and emitter region(s). For a sample with a base resistivity of 3 Ωcm and two emitters of 100 Ohm/sq on either side, yielding Gtot=0.028 Ω^{-1}/sq, the measured peak temperature was found to be 150°C higher than that of a 'bare' (lifetime) sample of 10 Ωcm with Gtot=0.0016 Ω^{-1}/sq.

Peer review by the scientific conference committee of SiliconPV 2015 under responsibility of PSE AG

Keywords: Firing, conveyor belt furnace, free carrier absorption, solar cells, lifetime measurement, Planck distribution, black-body radiation

1. Introduction

Firing with a conveyor belt infrared furnace is the last step in the manufacturing process of industrial silicon solar cells. In such a belt firing furnace, cells with screen printed metal contacts are positioned on the belt and the belt moves underneath or in between infrared heaters. Usually the belt furnace is divided into a number of zones where the power of the IR heaters of each zone can be set to a desired power output or to a desired temperature. The

Peer review by the scientific conference committee of SiliconPV 2015 under responsibility of PSE AG
doi:10.1016/j.egypro.2015.07.096

temperature is measured with thermocouples inside the firing furnace and through an electronic feed-back loop the power is adjusted to obtain the set ambient temperature in the firing furnace.

During the firing process the metallic contacts are formed. Contact formation is determined by intricate physical and chemical processes of migration of metallic particles, interaction of metallic particles with silicon as well as interaction of metallic particles and glass frit with dielectrics. For aluminum paste used on the rear side of standard industrial p-type solar cells processes like dissolution of silicon in molten aluminum, aluminum and silicon diffusion as well as recrystallization of silicon, denoted as epitaxial growth, leading to the well-known Al-BSF [1], are the important physics processes.

At the same time the elevated temperature prevailing in the silicon solar cell during firing triggers processes like hydrogen diffusion inside or outside dielectric layers like a:SiN_x:H and Al_2O_3. Diffusion towards silicon can lead to hydrogen bulk passivation and the passivation of dangling bonds at the surface. Effusion to the ambient results in hydrogen depletion. For Al_2O_3 or Al_2O_3-SiNx layers hydrogen migration is known to lead to blister formation of the dielectric layer [2]. At the same time elevated temperatures can lead to re-arrangement of atoms of the dielectric layer and the silicon surface thereby possibly changing the density of surface states and the surface charge of the dielectric layer. This the will affect the surface passivation quality of the dielectric layer.

In photovoltaics R&D a firing parameter study on either solar cells, samples or half-fabricates is an important instrument to optimize solar cell performance and to investigate phenomena like contact formation, Aluminum BSF formation, surface passivation and bulk passivation as a function of temperature. Often half-fabs (e.g. solar cells without metallization) and samples (e.g. symmetric structures with double-sided diffusions or a dielectric layers double-sided deposited) are manufactured and subjected to a firing study.

Many research papers report solar-cell characterization parameters like effective lifetime, recombination current density $j_{0,}$ or implied-V_{oc} as a function of firing temperature. However, quite often one implicitly refers to the firing *set*-temperature of the hottest zone, rather than the *measured* peak temperature. It is evident that these parameters are different and the measured temperature can deviate substantially from the set-temperature. One of the most obvious parameters that determines the difference between set and measured peak temperature is the belt speed.

The heat transfer inside a firing furnace is determined by conduction, between air and wafer, and between wafer and belt, and by absorption of IR radiation. In this work we do not aim to set up a full model that quantifies the prevailing temperature on a wafer during the firing process. Rather we show some experimental results illustrating how cell properties like surface morphology and doping level affect the temperature on the wafer. In addition we present some theoretical building blocks for a future model that illustrates the underlying physics. We will show that absorption of IR radiation in the silicon wafer plays a key role. We describe the absorption rate of radiation in a wafer by analytic means and we derive a formula for the absorption coefficient of IR radiation.

Nomenclature

IR	Infrared
BSF	Back Surface Field
FCA	Free Carrier Absorption
RP	Random Pyramids

2. Physics of IR radiation heat transfer to wafers

In this work we assume that absorption of IR radiation is the dominant factor for the heating up of wafers in a belt firing furnace. This holds particularly when the silicon wafer has little contact with the belt. The belt is expected to be a bit colder than the wafer due to its big thermal mass. This can sometimes be witnessed as belt marks in photoluminescence pictures. Nowadays conveyer belts exist that ensure only little contact of the wafer with the belt. Examples are belts where the wafer rests on typically five dimples or V-shaped belts where the wafer only contacts the belt at the wafer edges.

2.1. Heat management

To first approximation an IR heater can be described as a black body that emits radiation according to Planck's law, where the radiation spectrum is given by

$$B(\lambda,T) = \frac{2hc^2}{\lambda^5} \frac{1}{e^{\frac{hc}{\lambda k_B T}} - 1} . \tag{1}$$

Figure 1 shows the Planck-spectra for temperatures that are representative for firing furnaces.

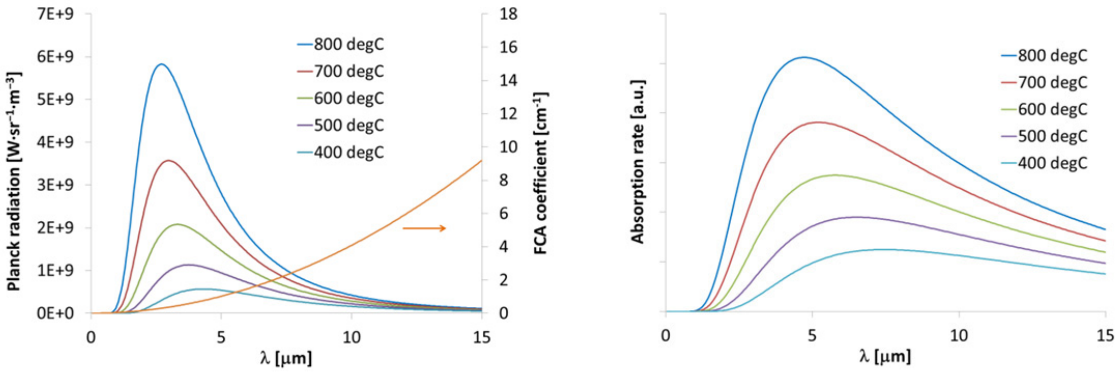

Figure 1 a) Planck black-body radiation as a function of wavelength, for different temperatures that are representative for heaters in a firing furnace. The brown curve represents the FCA coefficient for 1 Ωcm p-type silicon. b) The absorption rates computed as the Planck-spectrum weighed absorption coefficient. This can be interpreted as the FCA rate for black-body radiation in an infinitesimally thin wafer.

Silicon is well known of its capability to absorb electromagnetic radiation with energies above the band-gap, which corresponds to wavelengths below 1.1 um. As can be seen from Figure 1 the radiation below 1.1 um of the Planck spectra is virtually zero, indicating that the heating up of a solar cell in a firing furnace due to band-gap absorption is expected to be negligible. On the other hand IR radiation, with wavelengths bigger than the band-gap wavelength are dominant. Free carriers present in the semiconductor are known to absorb IR radiation [3].

2.2. Free Carrier Absorption

Free Carrier Absorption (FCA) is derived from Drude's simple model for the harmonic oscillation of unbound electrons in a fixed array of scattering nuclei. According to the Drude's model the absorption coefficient α [cm^{-1}] for electromagnetic radiation is

$$\alpha(\lambda) = Kc\lambda^2 . \tag{2}$$

Here, c stands for the free carrier concentration in cm^{-3} and λ is the wavelength of IR radiation in cm. According to [4] the Drude constant K equals $2.7 \cdot 10^{-10}$ and $1.0 \cdot 10^{-10}$ for p-type and n-type, respectively. In silicon the Free Carrier concentration is equal to the concentration of the majority carriers, at temperatures where solar cells are operated. The majority carrier concentrations are $p=N_A$ for p-type and $n=N_D$ for n-type. However, for elevated temperatures the majority concentration is derived from combining the charge neutrality condition $p\text{-}n\text{-}N_A=0$ (we restrict ourselves to p-type) and the equation for the mass action law for semiconductors $np=n_i^2$, where n_i is the intrinsic carrier concentration. This then results in

$$C(T)=\frac{1}{2}\left(N+\sqrt{N+4n_i^2(T)}\right) \tag{3}$$

Here, C is the hole/electron concentration and N is the acceptor/donor concentration for respectively p-type and n-type material. An expression for n_i^2 can be found in many text books. For brevity we use a form that is relative to the quantities at room temperature, denoted with the zero-subscript.

$$n_i^2(T)=n_{i,0}^2\left(\frac{T}{T_0}\right)^3 \exp\left[\frac{E_g}{k_B T_0}(1-\frac{T_0}{T})\right] \tag{4}$$

Here, $n_{i,0}^2=10^{20}$ cm^{-3}, E_g is the energy of the bandgap, k_B is Boltzmann's constant and $E_g/(k_B T_0)=43.6$. The majority concentration C as a function of temperature is depicted in Figure 2.

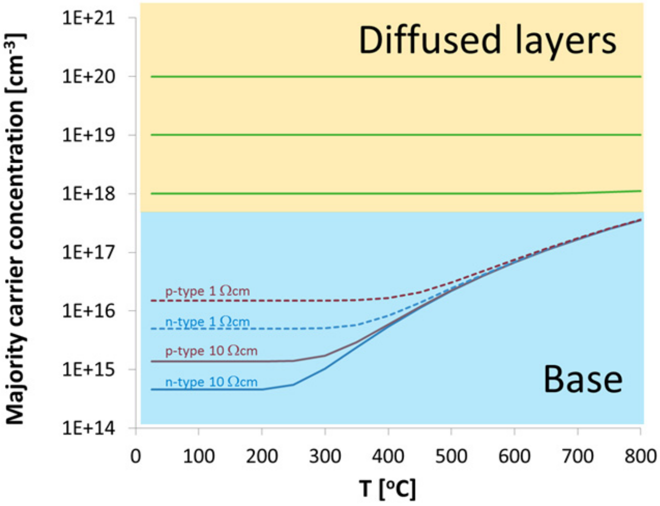

Figure 2 Majority carrier concentration as a function of temperature for a number of doping concentrations that are representative for the silicon material bulk (i.e. base) and for diffused layers. For diffused layers the majority carrier concentration is independent of the temperature, whereas for doping concentrations prevailing in bulk material a strong temperature dependence is visible.

The curves in the bottom half plane mark majority concentrations 'boundaries' from 1 to 10 Ωcm that are representative for the base of a solar cell, and are depicted for both p-type and n-type. From the curve-terminals at room-temperature the corresponding doping concentration can be read. Here, $C=N$ holds. The curves show that for temperatures between 250 and 400 °C, depending on material type and resistivity, the majority concentration starts to deviate from the $C=N$ limit and makes a transition to the other limit, namely $C=n_i(T)$. This shows that the FCA becomes more effective in the base when the temperature increases beyond 250-400 °C. Note that at these high temperatures the *minority* carriers also approach n_i and also start to contribute to the FCA. Hence the total FC concentration tends to $2n_i$. The upper half plane of Figure 2 shows typical concentrations present in diffused layers. Here, it becomes clear that for diffused layers, the majority concentration is not affected by temperature and hence $C=N$ is valid.

2.3. FCA absorption

The absorption of IR radiation in a wafer, for one pass in the perpendicular direction, is given by $A=1-\exp(-\alpha(\lambda)d)$, where d is the wafer thickness. By combining this expression with equations (2), (3) and (4), one obtains the absorption per wavelength.

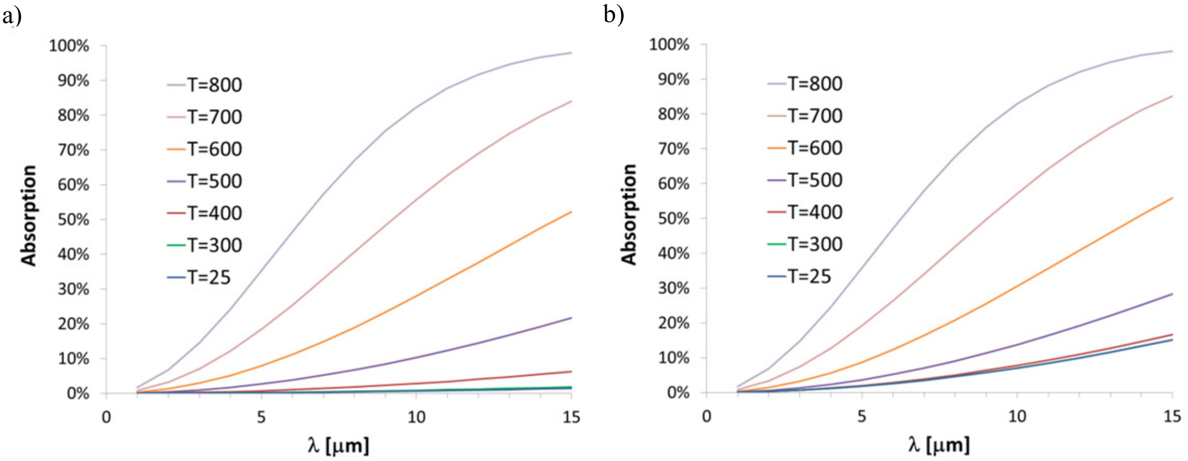

Figure 3 Absorption percentages of IR radiation as a function of wavelength, with the wafer temperature in °C as parameter. The absorption refers to IR radiation of one pass through a p-type wafer of thickness 180μm. The picture left shows a) 1 Ω cm and right b) 10 Ω cm corresponding to the curves with red labels in Figure 2.

Figure 3 shows the one-pass absorption rate for p-type wafers with d=180μm. At low temperatures, i.e. T < 400 °C a difference can be seen between 1 and 10 Ωcm, as one would expect of the curves in Figure 2. At wavelengths between 2 and 4 um where the Black Body radiation shows a maximum (see Figure 1.a) the absorption is below 30%, illustrating that the wafers are quite transparent for the most important part of the spectrum. It should be noted that for n-type material the wafer is even more transparent to IR radiation. The reason of this is twofold. Firstly the majority carrier concentration (at low temperature) is lower than for p-type with same resistivity and secondly the parameter K in eq.(2), is nearly three times smaller.

2.4. Planck-weighed absorption coefficient.

The product αd is low for the dominant wavelengths of the Planck radiation curve, implying that the absorption is weak and that the absorption profile is quite flat. As mentioned before this is particularly the case for low wafer temperatures as well as for diffused layers. Moreover, the reflection is constant for wavelengths beyond 1 μm and hence the wavelength distribution of the black-body radiation that enters the wafer is conserved. In the thin-slab approximation we can write the one-pass absorption as follows

$$A=\int_0^\infty B(\lambda,T_{BB})\left[1-\exp(-\alpha(\lambda,T_w)d)\right]d\lambda \approx d\int_0^\infty B(\lambda,T_{BB})\alpha(\lambda,T_w)d\lambda \qquad (5)$$

Here, T_{BB} stands for the temperature of the black body radiation and T_w for the wafer temperature. In the thin-slab approximation, we can identify the following, wavelength-independent, absorption coefficient for black-body radiation:

$$\alpha_{BB}(T_{BB},T_w)=\frac{\int_0^\infty B(\lambda,T_{BB})\alpha(\lambda,T_w)d\lambda}{\int_0^\infty B(\lambda,T_{BB})d\lambda} \tag{6}$$

By inserting eq.'s (1) and (2) in this equation we obtain:

$$\alpha_{BB}(T_{BB},T_w)=K\cdot C(T_w)\frac{\int_0^\infty \lambda^{-3}\left(e^{\frac{hc}{\lambda k_B T_{BB}}}-1\right)^{-1}d\lambda}{\int_0^\infty \lambda^{-5}\left(e^{\frac{hc}{\lambda k_B T_{BB}}}-1\right)^{-1}d\lambda}=K\cdot C(T_w)\cdot\left(\frac{hc}{k_B T_{BB}}\right)^2\frac{\int_0^\infty y^{-3}\left(e^{1/y}-1\right)^{-1}dy}{\int_0^\infty y^{-5}\left(e^{1/y}-1\right)^{-1}dy} \tag{7}$$

Evaluating the definite integrals [5] gives:

$$\alpha_{BB}(T_{BB},T_w)=B\frac{K\cdot C(T_w)}{T_{BB}^2} \tag{8}$$

where the constant *B* reads

$$B=\frac{5}{2\pi^2}\left(\frac{hc}{k_B}\right)^2=0.5244 \tag{9}$$

So, here we have arrived at a universal expression for Drude-model based FCA of black-body radiation in thin slabs. This equation is valid for one carrier type. The equation can be generalized for semiconductor thin slabs to account for both minority and majority carriers and then becomes

$$\alpha_{BB}(T_{BB},T_w)=B\frac{K_{ma}C(T_w)+K_{mi}\dfrac{n_i^2(T_w)}{C(T_w)}}{T_{BB}^2} \tag{10}$$

where K_{ma} and K_{mi} are the Drude-constants for the majority and minority carriers, respectively.

Figure 4 shows the Black-body absorption coefficient for a thin silicon wafer (blue and red curves) as well as for thin diffused layers with $10^{18} < N\,[\mathrm{cm}^{-3}] < 10^{20}$. Although for the latter α_{BB} is much higher, the product $\alpha_{BB}\cdot d$ is much less than unity since the diffused layer thickness *d* is usually <0.5 µm . Also for the bulk $\alpha_{BB}\cdot d < 1$ and therefore the thin-slab approximation seems justified for both wafers and diffused layers, and hence also for solar cells.

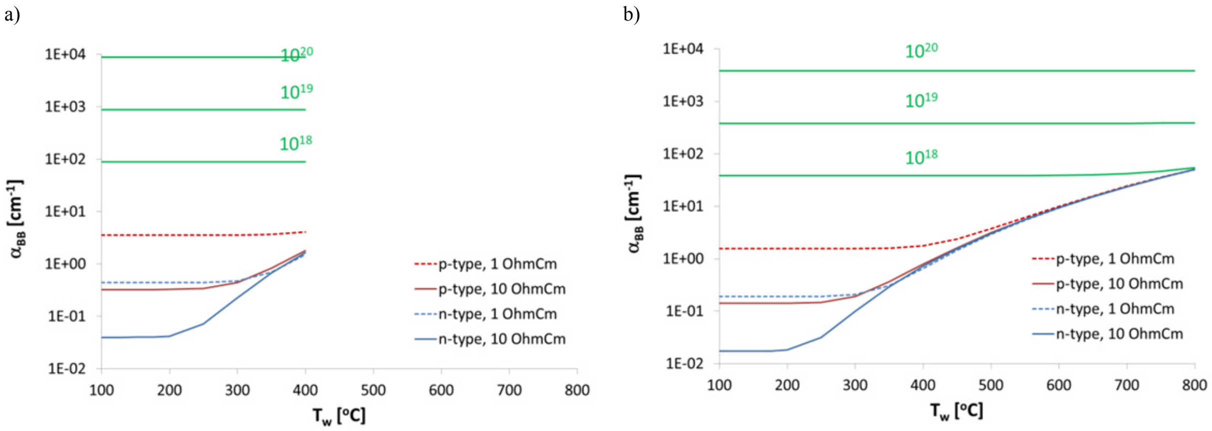

Figure 4 Black-body absorption coefficient as a function of wafer temperature for wafer bulk conditions (blue and red) as well as for n-type diffused layers (green curves). The black-body temperature is 500 °C left (a) and is 800 °C right (b).

2.5. Theoretical building block for a heat transfer model.

It is not the intention of this paper to present a comprehensive model that describes the heating up of solar cells in firing furnaces. Yet we present a theoretical building block for setting up such a model in the future. Since we have derived the thin-slab black-body absorption coefficient we can derive a dynamic heat equation that describes the change in temperature as a result of a the absorption by the thin wafer of the prevailing black-body radiation field, characterised by temperature T_{BB}. According to Stefan-Boltzmann's law the total power emitted per unit area of a black body equals σT^4, where the Stefan-Boltzmann constant in Js^{-1}cm^{-2}K^{-4} reads

$$\sigma = \frac{2k_B^4\pi^5}{15c^2h^3} = 5.67\cdot 10^{-12} \tag{11}$$

In a firing furnace the wafer receives radiation from the IR heaters. Clearly the IR heaters that are above and underneath the cell are most effective in transferring their heat to the wafer. If the space in between the top and bottom IR heater is narrow compared to the wafer size, the wafer will view a heater area that is twice as big as the wafer area (top plus bottom). Let us introduce an effective radiative area *ma*, where *a* is the cell area and where *m* is an effective area enhancement factor that can be computed exactly by integrating over spherical angles accounting for al radiances in the surrounding furnace materials (see [6]). For a narrow space and equal bottom and top heaters, *m* will tend to two. Using this definition we can write for the change of wafer temperature per unit of time due to absorption of radiation the following equation

$$\frac{dT_w}{dt} = \frac{ma\sigma T_{BB}^4(t)}{C_h ad}\cdot(1-R)\cdot\alpha_{BB}(T_{BB}(t),T_w(t))\cdot Zd \tag{12}$$

Here, C_h = 1.64 Jcm^{-3}K^{-1} is the heat capacity of silicon, *d* is the wafer thickness, *R* is the external reflection of IR radiation at the wafer surface and *Z* is the path length enhancement factor of radiation that has entered the wafer due to internal reflections. Note that the term αZd represents the absorption rate of IR radiation once entered the wafer. Clearly the wafer thickness determines both the amount of energy absorbed per unit of time but the heat capacity of the wafer in terms of J/K/wafer also scales with the thickness. This implies that, the temperature increase of the wafer due to radiation absorption is independent of the thickness, provided that the thin-slab approximation holds.

Likewise a bigger area *a* means both more IR radiation absorbing area but also more heat capacity due to a bigger size. Both *a* and *d* cancel in the equation and therefore we can write

$$\frac{dT_w}{dt} = \frac{m\sigma T_{BB}^4(t)}{C_h} \cdot (1-R) \cdot \alpha_{BB}(T_{BB}(t), T_w(t)) \cdot Z \tag{13}$$

By combining eq.'s (9) , (10), (11) and (13) we obtain

$$\frac{dT_w}{dt} = \frac{m}{C_h} \frac{\pi^3 k_B^2}{3h} T_{BB}^2(t) \cdot (1-R) \cdot \left[K_{ma} C(T_w) + K_{mi} \frac{n_i^2(T_w)}{C(T_w)} \right] \cdot Z \tag{14}$$

This nonlinear first-order differential equation, can be solved for $T_w(t)$. The term $T_{BB}(t)$ should be seen as source term determined by the belt speed and the temperature settings of the heaters in the furnace. Until so far the wafer has been considered as a radiation absorbing object in a thermal field omitting the emission of radiation by the wafer. It should be noted that a more comprehensive model is needed to describe precisely the temperature dynamics of the wafer in a belt firing furnace. Also the heat transfer by conduction as well as the emission of radiation of the wafer to the surroundings should be included [7].

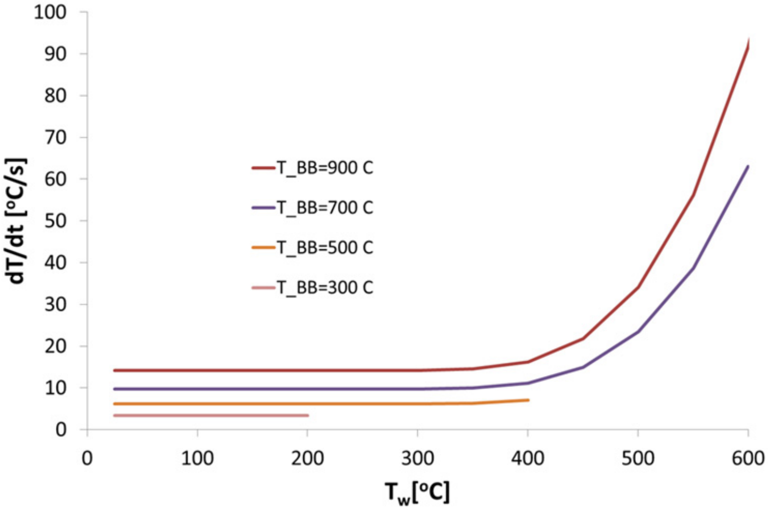

Figure 5 Wafer temperature increase per unit of time according to eq.(14) where m=2, Z=1, R=30% for a 1 Ω cm p-type wafer.

Figure 5 shows the temperature increase per unit of time as a function of wafer temperature for a 1 Ωcm p-type wafer, with the Black-body temperature of the IR heaters as a parameter. At low wafer temperatures, when the free carrier concentration equals the doping concentration, the temperature increase is independent of the wafer temperature and relatively small. For elevated temperatures, where the concentration of both carrier types tends to n_i, the temperature gradient increases and a super linear temperature profile as a function of time can be expected. The spaces between the curves illustrates the effect of enhanced absorption that scales with the black-body temperature squared.

3. Experimental results

A variety of p-type samples have been processed in our laboratory. These samples differ in surface morphology (iso textured, RP textured or polished), in coatings (Al_2O_3, SiNx, or bare), in base resistivities and in the presence or absence of emitters. All samples were fired in an industrial Despatch conveyer belt firing furnace. The eight heat zones had the following set-temperatures: 100, 100, 120, 200, 310, 600, 775, 975 ^{o}C and the belt speed was 200 inch per minute. The samples were placed directly on the belt (rather than on the dimples). The temperature on each sample was measured with two thermocouples using a Datapaq-profiler [8], [9].This measurement was done twice per sample. Figure 6 shows for three samples how the measured T-profiles look like and reveals that a temperature difference of about 150 ^{o}C can be observed between two high-Ohmic samples of which one has RP texture and the other has a polished surface. Here, the mentioned difference of IR radiation coupling of ~30%-rel in favour of RP texture becomes visible. The difference between the red and the green curve of about 100 ^{o}C for the peak temperature shows the impact of a higher doping level due to a lower base sheet resistance and due to the presence of two emitters.

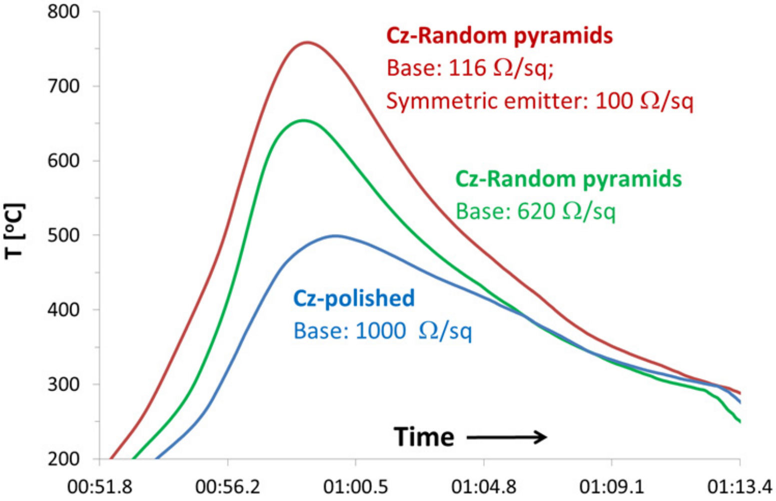

Figure 6 Datapaq temperature profile for three different samples showing the impact of surface morphology and doping level on peak temperature. All samples have been fired with the same firing settings.

It should be noted that at t≈00:53 the temperature difference between the red and green curve is already 50^{o}C. This can be ascribed to the doping level, since at this temperature the free carrier concentration in the bulk is still equal to the doping concentration as can be seen from Figure 2. Table 1 shows the properties of all samples. The second last column shows the parameter $G_{sh,tot}$ which is the total sheet conductance. It is the summation of the sheet conductance, i.e. $1/R_{sh}$, for the diffused layers and the base. The last column shows the measured peak temperature of the sample.

Table 1. Measured peak temperature of variety of samples all fired with heat zone 8 set to 975°C and a belt speed of 200 inch per minute. Surface morphology: Iso=iso texture, Pol=acid polished, RP=random pyramid texture

Surface	Coating	Base Rsh [Ω/sq]	Emitter Rsh [Ω/sq]	Gsh,tot [mS/sq]	Tpeak[°C]
Iso-Iso	-	113	-	9	670
	SiNx-SiNx	91	100 (2x)	31	775
	Al_2O_3-Al_2O_3	91	-	11	742
Pol-Pol	-	120	-	8	636
	-	153	-	6.5	603
	-	261	-	4	594
	-	1000	-	1	503
	SiNx-SiNx	153	-	6.5	643
RP-RP	-	161	-	6	695
	-	277	-	4	700
	-	620	-	1.6	648
	SiNx-Al_2O_3	130	77	21	763
	SiNx-SiNx	116	100 (2x)	29	790
	SiNx-SiNx	161	-	6	725
	Al_2O_3-Al_2O_3	116	-	9	753

3.1. Total sheet conductance as dominant parameter

Figure 7 shows the peak temperature as a function of the total sheet conductance $G_{sh,tot}$. Clearly the effect of enhanced FCA is visible due to an increased total sheet conductance. Also the off-set between RP-texured and polished samples is visible.

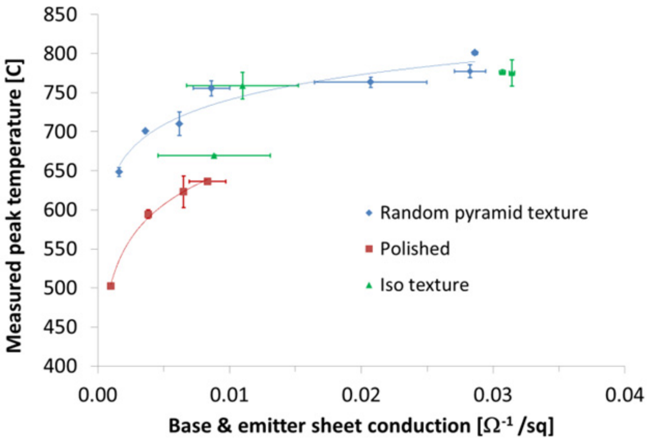

Figure 7 Measured peak temperature as a function of the total sheet conductance $G_{sh,tot}$ for all samples listed in Table 1.

Figure 7 reveals that the G_{tot} parameter is a good parameter for a crude interpolating for the prevailing sample temperature obtained in a firing furnace if the measured temperatures are known for a couple of G_{tot}-values, for a given furnace setting. However, a more comprehensive model, perhaps based on the presented theoretical building blocks, is needed to do this in an accurate way.

4. Discussion

Often R&D samples are fired at the same furnace settings as the corresponding solar cells. However, apart from the absence of metallization, these samples have different properties than the corresponding cells. The differences relate to surface morphology, fewer or more diffused layers, different bulk doping and different coatings. In order to measure for instance the recombination current with a photo-conductance lifetime measurement [10, 11, 12] it is recommended to measure at an injection level that equals 10 times the acceptor density, in case of p-type. To prevent uncertainties in mobility models and to prevent a big deviation between the average injection level and that at the sample boundary, wafers with resistivities of 10 Ωcm (p-type) are recommended. With such a high-Ohmic sample the surface recombination current j0 can be extracted from experimental data. However, if one is interested in this parameter for instance to understand the losses of the corresponding solar cell with a base of 1 Ωcm and if the lifetime sample is fired at the same setting as the solar cell we know that the parameters extracted from the lifetime sample measurement are not representative for the cell.

As an example we consider ECN's p-Pasha solar cell [13]. This cell has an emitter on the textured front side with a SiNx antireflection coating. On its rear it has a planar surface with an Al_2O_3 passivating coating and a screen printed Aluminum-paste grid. If one would be interested in the passivation quality of the Al_2O_3 layer, one would typically make a 10 Ωcm sample with, double-sided polished, surfaces coated with Al_2O_3. If one would fire this sample at the set temperature of the corresponding cell, having a 1 Ωcm base, this will lead to a much lower temperature, because of the reduced FCA due to the absence of an emitter and due the much lower base doping level. In addition the FCA will be reduced because of the increased reflection due the presence of two planar surfaces. Since the passivating quality of Al_2O_3 layers might decrease with increasing wafer temperature this would give an over-estimation in the lifetime measurement and would therefore present a distorted picture of the state of the solar cell.

Another relevant case is the following. The resistivity across an ingot is not always uniform. Especially for an n-type ingot the resistivity ranges typically from 2 to 11 Ωcm, which can be ascribed to the low segregation coefficient for phosphorus. The current study has demonstrated the impact of difference in base resistivity on the peak temperature reached in firing furnaces. This has been done on p-type wafers, but the same effect for n-type material can be expected. We expect a stronger effect of the base resistivity if the diffused layers are more lightly doped and also, if the diffused areas are smaller. For instance, n-PERL cells are expected to show a stronger sensitivity to base doping level than n-PERT cells. In industrial lines one could cope with this by adjusting the furnace set temperature based on a doping level entrance measurement. This could be performed by an IR laser transmission measurement and this could potentially lead to higher average efficiencies in factories. However, before implementing the suggested solution more research should be conducted to study the impact of the base resistivity on the heating of n-type cells in firing furnaces and to estimate the magnitude of the problem.

5. Conclusion

We presented a building block for a model to describe the heating up of solar cells and samples in belt firing furnaces. This building block deals with the absorption of IR radiation by Free Carrier Absorption. An analytically derived formula is presented for the absorption coefficient of a thin semiconductor slab present in a Planck spectrum. The absorption coefficient is inversely proportional with Black-body temperature squared. The absorption coefficient is furthermore proportional with the free carrier concentration. For diffused layers this concentration is independent of temperature. For the bulk material the free carrier concentration depends on temperature; at low temperature it is equal to the doping concentration and beyond 250-400 ^{o}C it is approaching twice the intrinsic carrier concentration n_i. Expanding the model and verification of it against experimental data is considered as future work.

We have shown in an experiment with different samples that measured peak temperatures on samples strongly depend on surface morphology and total doping level. A sample with random pyramid (RP) textured surface reached a 150 ^{o}C higher peak temperature, measured by thermocouples, than its counterpart with a polished surface. This can be ascribed to a 30% higher IR radiation coupling, indicating the importance of heat transfer by radiation in the firing furnace. We furthermore identified that the total sheet conductance, i.e. the summation of conductance of the diffused layers and of the bulk, is an important parameter for the heating up of the solar cell. A sample with a total sheet conductance of 26 mΩ^{-1}/sq, with contributions of the base and two emitters, showed a 100°C higher peak temperature than one with 1mΩ^{-1}/sq.

Acknowledgements

We acknowledge the financial support for the TKI project Pamplona by the Dutch authority RVO. We thank Pi Danzl for performing the Datapaq measurements.

References

[1] Th. Lauermann, B. Fröhlich, G. Hahn and B. Terheiden, "Diffusion-based model of local Al back surface field formation for industrial passivated emitter and rear cell solar cells", Prog. Photovolt: Res. Appl. 2015; 23:10–18.

[2] L.E. Black et al, "Thermal stabilityof silicon surface passivation by APCVD Al2O3", Solar Energy Materials & Solar Cells 120 (2014) 339–345.

[3] Simeon C. Baker-Finch, Keith R. McIntosh, Di Yan, Kean Chern Fong, and Teng C. Kho, "Near-infrared free carrier absorption in heavily doped silicon", Journal of Applied Physics 116, 063106 (2014).

[4] D. K. Schroder, R. N. Thomas, and J. C. Swartz, "Free carrier absorption in silicon," IEEE J. Solid State Circuits SC-13(1), 180–187 (1978).

[5] I.S. Gradshteyn and I.M. Ryzhik, Table of Integrals, Series, and Products, 2007, Elsevier Inc.

[6] B. Lu, L. Zongcun, and S. Hui, "Thermal Field Analysis and Simulation of an Infrared Belt Furnace Used for Solar Cells", International Journal of Photoenergy (2014), Article ID 391270. .

[7] R. Kakoschke, E. Bussmann, H. Föll. "Modelling of wafer heating during rapid thermal processing.", Applied Physics A Solids and Surfaces, 50 (2) p.141 (1990).

[8] J. Hoornstra, A. van der Heide, J. Bultman, and A. Weeber, "Simple, detailed & fast firing furnace temperature profiling for improved efficiency," in Proceedings of the Conference PV in Europe—From PV Technology to Energy Solutions, p. 276, 2002.

[9] www.datapaq.com

[10] Kane DE, Swanson RM. Measurement of the emitter saturation current by a contactless photoconductivity decay method (silicon solar cells). Proceedings of the 18th IEEE Photovoltaic Specialists Conference, 1985; 578–583.

[11] Sinton Instruments, WTC120 manual

[Green] M. A. Green, Silicon Solar Cells: Advanced Principles and Practice (University of New South Wales, Sydney, Australia, 1995), p. 45, 48-49.

[12] H. Mäckel, K. Varner, On the determination of the emitter saturation current density from lifetime measurements of silicon devices, Progress in Photovoltaics: Research and Applications, 21 (2013) , 850-866.

[13] I. Cesar et al, "Efficiency Gain For Bifacial Multi-Crystalline Solar Cell With Uncapped Al2O3 and local Firing-through Al-BSF.", 39th IEEE Photovoltaic Specialists Conference, 2013, Tampa.